Improvement of solar irradiance modelling during cloudy-sky days using measurements

Léa Al Asmar, Luc Musson Genon, Eric Dupont, Jean Charles Dupont, Karine Sartelet

Version of Record: https://www.sciencedirect.com/science/article/pii/S0038092X21009488
Manuscript_6351ec43e8a06cce9354bb3e84a17800

Improvement of solar irradiance modelling during cloudy-sky days using measurements

Léa Al Asmar[a], Luc Musson-Genon[a], Eric Dupont[a], Jean-Charles Dupont[b], Karine Sartelet[a]

[a]*CEREA, Joint Laboratory Ecole des Ponts ParisTech-EDF R&D, 6 Quai Watier, 78400 Chatou cedex, France*
[b]*LMD, Palaiseau, France*

Abstract

Clouds have a strong influence on the amount of solar irradiance reaching the ground. However, they have large spatio-temporal variations and are difficult to model. The 1D irradiance model of code_saturne is used to estimate the global and direct solar irradiances at the ground, taking into account the impact of atmospheric gas, clouds and aerosols. Simulations are conducted and compared to measurements at the French SIRTA observatory (instrumental site for atmospheric remote sensing research), located in Palaiseau, Ile-de-France in August 2009 and in the year 2014. Although irradiance is very well modelled during clear-sky days, it is over-estimated during cloud-sky days. The estimation of irradiance during cloudy-sky days is improved by coupling the model to on-site measurements of cloud parameters from the SIRTA. RMSEs around 59 W m^{-2} and 50 W m^{-2} and MBEs around +17 W m^{-2} and -18 W m^{-2} are obtained, respectively, for global and direct irradiances during cloudy-sky days using pyranometer measurements for cloud fraction and microwave radiometric measurements for liquid water path. A sensitivity analysis on the cloud parameters that may lead to the best improvement of simulated irradiance is performed. The cloud optical depth is the most important one, followed by the cloud fraction. The different instruments used for the determination of these parameters are examined. Moreover, hourly values of solar fluxes are analysed to determine and physically understand persistent errors between model and measurements when measured cloud parameters are used.

Keywords: clouds, irradiance modelling, code_saturne, cloud optical properties, on-site measurements

1. Introduction

The energy transition is a pathway toward the decarbonisation of the energy sector. It is necessary to reduce energy-related CO_2 emissions to limit climate change. To do so, energy-efficiency measures and renewable energies are set up. Thus, the expansion of solar energies is an important cornerstone of the energy transition. Solar irradiance is the input power source of photo-voltaic (PV) generators. An accurate prediction of the amount of solar irradiance reaching the ground is necessary to reduce the uncertainty on PV energy-yield assessment, to optimize the performance of PV farms, and to forecast the production at different time scales. The amount of solar irradiance reaching the ground is influenced by different geographical, meteorological and atmospheric parameters. Those parameters have important spatio-temporal variations, leading to difficulties to accurately model solar irradiance.

Depending on the forecast needs, different models have been developed to represent irradiance fluxes at the surface of the Earth (Lorenz and Heinemann, 2012; Diagne et al., 2013). They can be categorized according to the forecasting timescales: for very short time scales (from minutes to few hours), statistical models combined to on-site measured irradiance data can be used (Reikard, 2009). Satellite or cloud-imagery based models are used to derive irradiance forecasts (Lorenz and Heinemann, 2012), but they highly depend on the data availability, which depends for example on the passage of the satellite over the studied area. For longer forecasting times (longer than some hours), Numerical Weather Prediction (NWP) models are the most suitable choice. NWP models are based on the modelling of physical phenomena. They predict the atmospheric variables based on current weather condition by solving the differential equations describing the evolution of these variables, which are required to estimate solar irradiance. Hybrid models have also been developed. They merge different approaches and derive an optimized forecast depending on the forecast horizon that integrates different kinds of input data (Cao and Cao, 2005).

NWP and hybrid models represent the diffuse, direct and global solar irradiances with different levels of complexity: from empirical models (Rigollier et al., 2000) or physics-based models (Xie et al., 2016) to radiative transfer based calculations (Müller et al., 2004) as presented in the overview of (Ine-

ichen, 2006). An example of an intermediate complexity representation is the two-stream approximation, which solves the transfer of irradiance through a plane parallel atmosphere and integrates irradiance over the zenith angle. Transmission and reflection functions are estimated using two or more spectral bands, and integrated over the vertical, like the rapid radiative transfer model (RRTM) (Clough et al., 2005) that uses the DIscrete Ordinate method for Radiative Transfer (DISORT) algorithm (Stamnes et al., 1988) to solve the radiative transfer equation using multiple scattering. In the physics-based model of (Xie et al., 2016), the cloud transmittance and reflectance is estimated using plain exponential functions of solar zenith angle, cloud optical thickness and effective particle size. The description of the state of the atmosphere is required as an input of these solar-irradiance models. Atmospheric parameters include the optical properties of aerosols (AOP), clouds, water vapor and other gases. Although meteorological parameters may be derived from NWP, this is not always the case for AOPs, which may be derived from chemical transport models (Breitkreuz et al., 2009; Sartelet et al., 2018).

The direct irradiance is crucial for the economic and energy evaluations of different solar energy applications, like solar concentrating and flate plate systems (Padovan et al., 2014). It can be estimated from the transmission functions in the intermediate complexity models presented above. In empirical models, its estimation can be quite complex and decomposition models based on observations are sometimes used to separate the direct normal irradiance (DNI) from global horizontal irradiance (GHI) (Padovan et al., 2014; Bertrand et al., 2015) or simple methods for correcting the satellite derived DNI data (Polo et al., 2015).

Clear-sky irradiance is often accurately modelled (Psiloglou and Kambezidis, 2007; Blanc et al., 2011; Lefèvre et al., 2013; Kambezidis et al., 2016; Sartelet et al., 2018), especially when the influence of aerosols is taken into account. Sartelet et al. (2018) (referred to as KS18) showed that irradiance fluxes at the surface are strongly improved during clear-sky days when AOP are estimated from the aerosol concentrations simulated by a chemistry-transport model.

However, the modelling of irradiance during cloudy-sky days is a common problem for the various numerical models (Morcrette, 1991; Morcrette et al., 2008; Lorenz and Heinemann, 2012; Diagne et al., 2013), KS18. Clouds have a strong influence on solar irradiance at the surface but they are extremely variable in space and time. The parameterisation of clouds requires the deter-

mination of the cloud fraction at the ground, which requires the knowledge of the overlapping of the different vertical cloud layers (Räisänen, 1998), as well as cloud optical properties such as cloud optical depth (COD), single scattering albedo, and asymmetry factor (Stephens, 1978; Stephens et al., 1984; Nielsen et al., 2014). In particular, low clouds are found in nearly all types of convecting systems and are misrepresented in climate models (Naud et al., 2010; Haynes et al., 2011; Gregow et al., 2020). Satellite measurements have been used to improve the representation of cloud properties and irradiance . For example, geostationary satellite-derived cloud properties have been used to derive surface solar irradiance under cloudy sky (Schillings et al., 2004). The brightness measurements from GOES satellite images have been used to derive the bulk effect of clouds, the cloud albedo and absorption (Gautier et al., 1980). To better forecast irradiance, different methods are used. The description of clouds and irradiance in NWP models may be improved using satellite and/or in-situ measurements and data assimilation, as detailed in (Kurzrock et al., 2018) and (Gregow et al., 2020): as satellite irradiances contain information on clouds, they may be directly assimilated; or retrieved cloud properties may be used to adjust the initial state of the NWP model. Other methods exists in literature. For example, in (Roy et al., 2001), a neural network approach is used to derive cloud coverage in the sky. In (Moncada et al., 2018), an artificial intelligence method is combined to sky imager data to forecast irradiance.

The goal of the current study is to improve the estimation of irradiance during cloudy-sky days by coupling a solar-irradiance model with on-site measurements, and to compare the added-value of different measurements. Because irradiance on cloudy-sky days is strongly influenced by the cloud fraction and the cloud optical depth (COD) (Lorenz and Heinemann, 2012), their representation using different parameterisations and measurements will be compared to determine the most efficient ones.

The 1D irradiance model included in the 3D CFD (Computational Fluids Dynamics) model code_saturne[1], described in KS18, is used in this study to represent the global and direct solar irradiances. Meteorological data from the WRF model and aerosol's concentrations from the air-quality modelling platform *Polyphemus* are used as input data (Sartelet et al., 2018; André et al., 2020). The measurements of cloud properties are obtained from dif-

[1]https://www.code-saturne.org/cms/

ferent instruments of the French observatory SIRTA (Haeffelin et al., 2005), located in the southern suburbs of Paris. The article is structured as follows: first, the methodology and configuration of the simulation are detailed. Second, the modelling of irradiance during clear-sky days and cloudy days is briefly evaluated. Third, the impact of using different measured parameters to improve the modelling during cloudy days is estimated. Finally, an analysis of errors conforming to cloud properties is presented.

2. Methodology

2.1. The solar irradiance scheme of code_saturne

code_saturne is an open source CFD software. It solves the Navier-Stokes equations for 2D, 2D-axisymmetric and 3D flows. In this study, the standalone 1D irradiance model of code_saturneis used to estimate, every hour, the total solar irradiance and its direct and diffuse horizontal components at the surface of the Earth (KS18).

This model parameterises the attenuation of irradiance from gas, aerosol and clouds present in the atmosphere above the location studied. The solar irradiance flux is computed by considering irradiance from two spectral bands: the ultraviolet–visible (UV–vis) band (300–700 nm) and the solar infrared (SIR) band (700–3000 nm). In these two spectral bands, the solar irradiance is influenced by different processes:

- In the UV-vis band, solar irradiance is absorbed by ozone in the stratosphere and is scattered by air molecules (Rayleigh scattering), aerosols and clouds in the troposphere.
- In the SIR band, the absorption by water vapour dominates the ozone absorption in the troposphere.

The calculation of the irradiance is done at the ground surface by calculating the attenuation in the column above the surface. For the global and direct irradiance, this attenuation absorption is estimated through reflection and transmission factors defined by the multiple-scattering theory using the two-stream approximation (LH74 (Lacis and Hansen, 1974)). The atmosphere is assumed to have horizontally homogeneous optical properties and gas concentrations. The reflection and transmission factors of LH74 are used with the optical properties of atmospheric components integrated over the

vertical axis. The original LH74 scheme has been modified to introduce the cloud fraction and differentiate the calculation during cloudy and clear-sky days, to compute both the direct and diffuse components of solar irradiance, and to take into account the aerosol contribution.

The description of the equations used here are similar to those of KS18, and are described in the appendix. The difference between KS18 and the present study lies in the calculation of the direct irradiance : in KS18, the parameterisation of (Psiloglou and Kambezidis, 2007) is used while the current study uses a formula that we derived and that is more consistent with the global irradiance model developed by LH74.

2.2. Input data

The solar irradiance scheme needs several inputs to be specified, such as the ground albedo and the vertical distribution of:

- Meteorological variables: temperature, pressure, relative humidity.
- Aerosol and cloud optical properties (optical depth, liquid water path (LWP), cloud cover fraction, single scattering albedo and asymmetry factor).

The simulations of direct, global and diffuse solar irradiances are performed and compared to measurements at the French SIRTA observatory, located at Palaiseau, in the southern suburbs of Paris (Haeffelin et al., 2005). The SIRTA observatory hosts the BSRN station of Palaiseau. Two periods are simulated: the period of 'August 2009', from 04/08/2009 to 28/08/2009, as in KS18, and the 'year 2014', from 08/01/2014 to 28/10/2014. The model's chain used is represented in Figure 1:
The input meteorological data (temperature, pressure, relative humidity) and ground albedo are obtained from WRF simulations. The cloud optical properties (cloud cover fraction, liquid water content) are derived from WRF outputs or from measurements. The air-quality platform Polyphemus provided the aerosol concentration data for the year 2014, as presented in the following section. The aerosol optical properties are extracted from measurements for the period of August 2009. The configuration of the simulation used to generate the data is now briefly summarised, as well as the observational data used as input of the irradiance scheme to improve the cloudy-sky irradiance simulations.

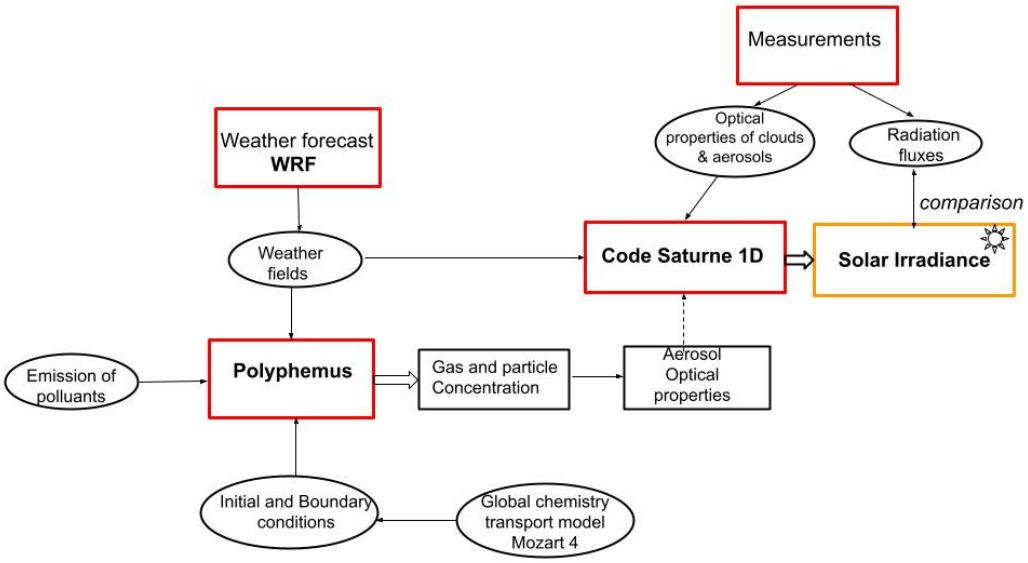

Figure 1: Scheme representing the models chain used for our cases of studies of August 2009 and the year 2014.

2.2.1. Simulated meteorological data

The input meteorological fields are obtained from simulations with the WRF model. WRF is an open-source mesoscale model that solves the compressible and non-hydro-static Navier-Stokes equations (Skamarock et al., 2008).

For August 2009, as detailed in KS18, the WRF model ran from 10 July to 30 August 2009 with hourly outputs. WRF simulations were initialized at 0000 UTC every 7 days with a 24 hours spin up. The simulation over the french domain was used for the current study. It has a spatial resolution of 20×20 km^2 (65 x 61 grid points), see Figure 1 of KS18. The vertical resolution goes from the surface up to 50 hPa. It is made of 40 terrain-following levels. The WRF "single moment 6 classes" scheme was used for the microphysics, combined with the Kain-Fritsch cumulus scheme ((Kain and Fritsch, 1993)).

For the year 2014, the set-up of the WRF simulation is detailed in (Sartelet et al., 2018). WRF simulations ran from 02 January to 28 October 2014 with hourly outputs. They were initialized at 0000 UTC every 6, 3 or 2 days depending on the period. The simulation over the greater Paris (Île-de-France) domain is used in the current study. Its spatial resolution is 5×5 km^2 resolution (41×41 grid points). The vertical resolution goes up to 100hPa and is made of 28 vertical levels refined near the surface. For miscrophysics, Kesseler scheme (Kessler, 1995) is used combined with the cumulus Grell-Freitas ensemble scheme (Grell and Devenyi, 2002).

Evaluation of the simulated ground albedo. The ground albedo is obtained from WRF simulations. For the period 'year 2014', the averaged simulated albedo is equal to 0.2 with a standard deviation of 0.02. The averaged measured albedo is equal to 0.13 with a standard deviation of 0.08. The use of measured albedo instead of simulated values in code_saturne doesn't impact solar irradiance calculations. Contrary to simulated values, the measured albedo depends on the zenith angle μ_0. For values of μ_0 for which irradiance is the strongest during the day, simulated albedo are similar to measurements.

2.2.2. Simulated aerosol concentrations

Aerosol optical data are computed using the air-quality modelling platform *Polyphemus* as detailed in KS18. The aerosol concentrations are computed with the chemistry-transport model Polair3D of the platform Polyphe-

mus, which also determined the size and the composition of particles. The meteorological data needed as input of Polair3D/Polyphemus were obtained by interpolating the WRF simulations detailed in the previous section on the Polair3D/Polyphemus grid. The set-up of the simulations is detailed in KS18 for August 2009 and in (Sartelet et al., 2018) for the year 2014. For August 2009, the simulations were performed from 15 July to 29 August 2009 over the France domain, with a spatial resolution of 0.2249° × 0.2249°ranging from latitude 41.2°N to 51.32°N and from longitude 5°W to 9.84 °E. The vertical was discretized with 8 levels of interfaces: 0, 50, 150, 300, 800, 1500, 2500, 4000, 6000 m. For the year 2014, the simulations were performed from 08/01/2014 to 30/12/2014 on the Île-de-France domain: spatial resolution of $0.02^o \times 0.02^o$ ranging from latitude 48°N to 49.5°N and from longitude 1.35°E to 3.55°E. The vertical was discretized with 14 levels of interfaces: 0, 30, 60, 100, 150, 200, 300, 500, 750, 1000, 1500, 2400, 3500, 6000, 12000 m.

Evaluation of the simulated AOD. For August 2009, as detailed in KS18: at 500 nm, the measured and simulated mean AODs are respectively 0.18 and 0.14 with a mean fractional error (MFE) of 43% and a mean fractional bias (MFBE) of -28%. For the year 2014, at 500 nm, the measured AODs from the SIRTA ReOBS (Chiriaco et al., 2018) and simulated mean values are respectively 0.056 and 0.07 with a MFE of 48% and a MFBE of +19 %. To evaluate simulations of particle concentrations, (Boylan and Russell, 2006) defined the following criteria: the MFE should be lower than 50 % and the MFBE should be between -30 % and + 30 %, which are well satisfied here. The AODs simulated by Polyphemus compare well to measurements.

2.2.3. Observational data at SIRTA

SIRTA is a French observatory dedicated to the observation of the atmosphere. It has been collecting data for more than 15 years from active and passive remote sensing instruments and in-situ measurements. It is located in a semi-urban area, 20 km south of Paris, France (48,71 °N, 2.2 °E). SIRTA Re-OBS is a project whose goal is to synthesize, analyze, homogenize, all SIRTA observations hourly averaged in a single NetCDF file from 2003 to now (Chiriaco et al., 2018).

Instruments and parameters

The instruments used and the parameters extracted from SIRTA Re-Obs are resumed in table 1.

Instrument	Variables	Uncertainty	Native Resolution	Availibilty	Reference
Multi-wavelength sun-photometer (CIMEL CE-318)	AOD by Sun and sky scanning	0.01	–	in 2009 and 2014	(Holben et al., 1998)
Pyranometers and Pyrheliometers (PYR)	Surface downwelling shortwave irradiance (global, direct and diffuse components); cloud fraction	-5 W m^{-2}	1s	in 2009 and 2014	(Long et al., 2006)
Sky imager	Cloud fraction	$\sim$ 5%; depends on cloudy situation	1min	in 2009 and 2014	(Long and DeLuisi, 1998)
Lidar	Cloud fraction (by integration over time); cloud base height	$\sim$ 5%	1h	in 2009	(Morille et al., 2007)
Meteosat Second Generation satellite	Cloud fraction (using the percentage of cloudy pixels over 15x15 pixels images); COD (in an iterative manner, by simultaneously comparing satellite-observed reflectances at visible and near-infrared wavelengths to lookup tables (LUTs) of simulated reflectances); LWP (from the retrieved COD and droplet effective radius)	–	3 km	in 2009	(Roebeling et al., 2006)
Microwave radiometer HATPRO	LWP	$\pm$ 20 g m^2	5s	in 2014	(Rose et al., 2005)
Celiometer	Cloud base height	15 m	30 s	in 2014	(Haeffelin et al., 2005)
Rain gauge R3070	Precipitation	0.1 mm	5s	in 2009 and 2014	(Haeffelin et al., 2005)

Table 1: Instruments and parameters extracted from SIRTA ReObs.

2.3. Determination of cloud properties

In order to represent clouds in the model, the cloud fraction and different cloud optical parameters (COP) are used: COD, which is presented in the following section, single scattering albedo, asymmetry factor, and cloud droplets effective radii, described in the appendix.

2.3.1. Cloud fraction

From WRF simulations. The simulated cloud fraction is known at each vertical level of the model. It is difficult to estimate the cloud fraction seen from the ground because the overlapping between cloud layers is not known. Here a maximum overlapping is assumed.

Comparisons of cloud fraction from satellite, PYR, sky imager and lidar in August 2009. The measured cloud fraction is integrated over the vertical. Cloud fractions issued from Meteosat Second Generation satellite data using the percentage of cloudy pixels are of great interest, because of their global coverage. However, data are only available when the satellite is passing above the studied location. Thus, the data extracted from satellite images is the one with the most invalid data ($\sim$ 28% of invalid values during the day). This percentage of invalid data is $\sim$ 10 % for the cloud fraction measured with a lidar, $\sim$ 7% for PYR, and 0% for the sky imager. The cloud fraction distribution in August 2009 obtained with these instruments is represented in the histogram of Figure 2a. In the set of values extracted from PYR and from satellite images there are respectively: $\sim$ 25 % and $\sim$ 32% of cloudy sky ($F_C > 0.95$), $\sim$ 25% and $\sim$ 18 % of clear-sky situations ($F_C < 0.05$) and $\sim$ 50% of partially cloudy-sky situations for both data sets. The data extracted from the sky imager does not contain values exactly equal to 0 or 1 but it contains , respectively, : $\sim$ 5 % and : $\sim$ 24 % of clear and cloudy sky situations.

Comparisons of cloud fraction from PYR and sky imager in 2014. For the year 2014, only the cloud fraction from PYR and from sky imager are available: the two set of data are quite similar with a RMSE score of 0.168, they are represented in figure 2b. The distribution of cloud fraction from PYR for the year 2014 is represented in Figure 3a and the box diagram for each season in Figure 3b. It should be noticed that in Autumn (October), 50% of the values of cloud fraction are equal to 1 and the other 50% are between 0.1 and 1. For the other seasons the median is around 0.85 in winter, 0.75

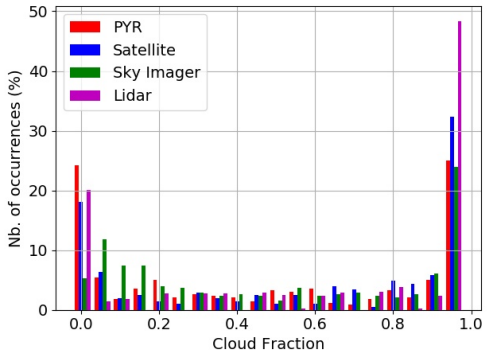

(a) Four different data sets are presented: cloud fraction from PYR, satellite images, sky imager and lidar.

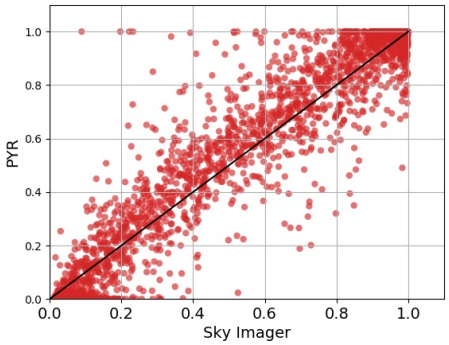

(b) Cloud fraction from PYR versus sky imager

Figure 2: Distribution of cloud fraction during August 2009 (a) and the comparison between the two available cloud fractions for year 2014 (b) at SIRTA.

in spring 0.82 in summer. Figure 3a represents the distribution of cloud fraction for each season, normalized by the number of valid values for each season. Over the whole year, fully cloudy situations (cloud fraction of 1) are the most frequent. The other values are in the range [0,0.99] with a higher density around 0. Therefore, there are only a few clear-sky situations and the distribution of cloud fraction is quite similar throughout the different seasons.

2.3.2. Cloud Optical Depth

The COD (τ_C) is an adimensional parameter that characterizes the strength of attenuation by clouds. When it is equal to 0, there is no extinction of irradiance due to clouds. τ_C depends on the type of cloud and the size of the water drops or ice crystals. For water clouds, it can be approximated by (Stephens, 1978):

$$\tau_C = \frac{3}{2}\frac{LWP}{\rho r_e} \tag{1}$$

where LWP is the liquid water path (g m^{-2}), ρ the density of water (g m^{-3}) and r_e the effective diameter in m.

From WRF simulations. When WRF simulations are used to estimate τ_C, it is calculated using equation (1) with LWP calculated with WRF and a

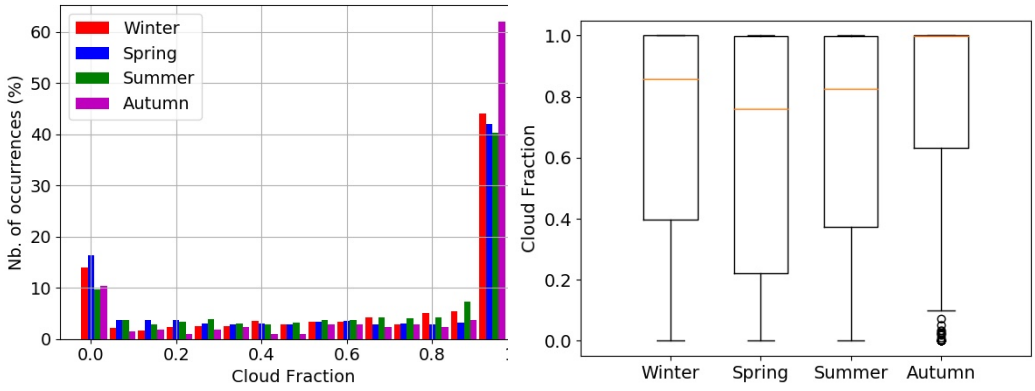

(a) Distribution

(b) Boxplot

Figure 3: The cloud fraction (PYR) at SIRTA during the four seasons of 2014.

constant value of r_e (14 μm (Stubenrauch, 2013)).

Satellite measurements of COD. They are available in the SIRTA ReObs data base for year 2009. The COD distribution is represented in the histogram of Figure 4b. The values range between 0 and 109 with a majority in the range [0,4]. Therefore, most of the clouds present at SIRTA are low density clouds (Stephens et al., 1984).

Microwave radiometer measurements of LWP. They are available for the year 2014 and their distribution is represented in Figure 4a. It can be seen that the LWP distribution is similar for the different seasons with most of the values lower than 25 g m^{-2}. The differences observed for autumn can be explained at least in part by the fact that autumn includes only October in this study. The variations of the LWP span a wider range of values when the cloud fraction is higher than 0.5 (Figure 5 shows the LWP versus cloud fraction in March and June, the evolution during these two months is well representative of the year). These high variations might be caused by the simultaneous occurrence of multiple cloud layers. Furthermore, the LWP increases with the cloud fraction.

Improvement of the estimation of COD from LWP. Because no estimation of COD and cloud droplet radii was available in 2014, the COD is calculated from the LWP data obtained from microwave radiometric measurements.

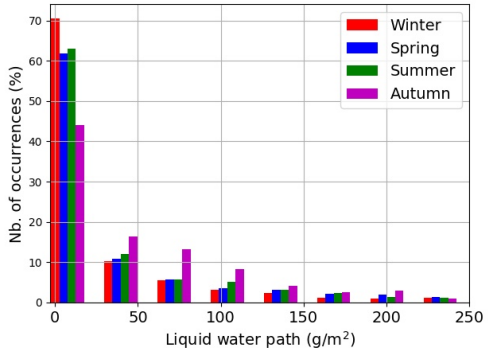

(a) Distribution of liquid water path from SIRTA microwave radiometric measurements according to the four seasons in 2014 (in g m^{-2})

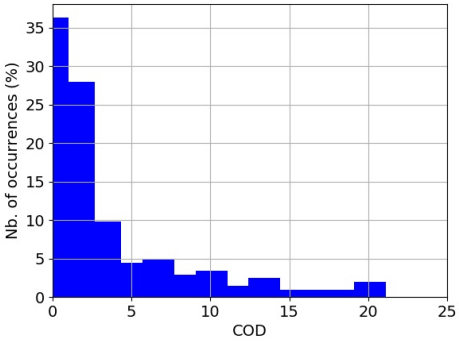

(b) Distribution of COD from SIRTA satellite measurements.

Figure 4: Distribution of COP in August 2009 and year 2014.

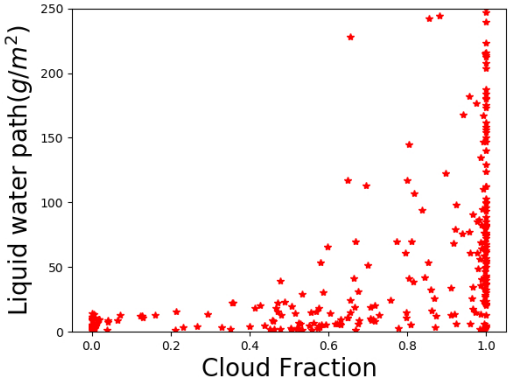

(a) March 2014

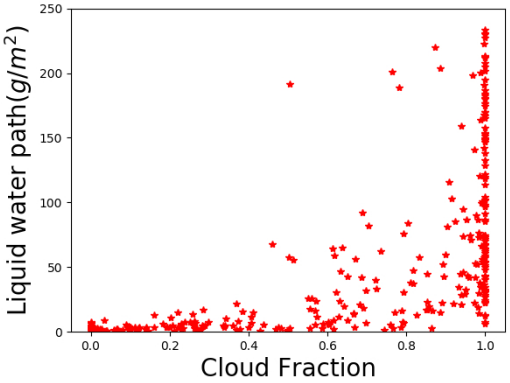

(b) June 2014

Figure 5: Distribution of LWP versus cloud fraction from PYR

To determine the relation between COD and LWP at SIRTA, satellite data from 2005 to 2010 are used. These data include values of COD and of LWP (which is derived from COD and from an estimation of the effective radius r_e following (Roebeling et al., 2006)). A first approach consisted in computing an averaged value of the effective radius over the whole period 2005-2010 (12 μm), and then to derive the COD for 2014 from the LWP measurements with equation 1 using this mean effective radius. As the effective radius varies in time, a second approach is to determine a statistical relation between COD and LWP using the satellite data from the period 2005-2010.

The relation between COD and LWP is fitted using two different equations, depending on the value of LWP:

1. A linear fit for values of the LWP lower than 14 g m^{-2}: $\tau_c = 0.181LWP - 0.001$ when $LWP \leq 14$ g m^{-2}
2. A logarithmic fit for values of LWP higher than 14 g m^{-2}: $log_{10}(\tau_c) = 1.7095ln(log_{10}(LWP)) + 0.2633$. This equation was inspired from the fitted equation of (Stephens et al., 1984) for conservative scattering because purely scattering is a good approximation for clouds for solar irradiance.

The scattering plot of COD versus LWP and the fitted models are represented in Figure 6a. The RMSE between the estimated COD and the measured one is calculated to compare the different models over the period 2005-2010. A RMSE of 8.18 is obtained with equation 1 and 7.6 with the relation established in this paper, which is the best approximation of COD for our specific case. The distribution of LWP for the period 2005-2010 shows that the majority of points are in a range of LWP going from 5 to 100 g m^{-2}(Figure 6b). The fitted model is then pushed by those values of LWP, it coincides well for our case: in 2014, the majority of LWP falls into the same range (Figure 4a).

2.4. Separation between clear-sky and cloudy-sky days

Due to the difficulties linked to the modelling of clouds, the model is evaluated separately for clear-sky days and cloudy-sky days. At the SIRTA, the separation between clear-sky days and cloudy-sky days is done using the measured cloud fraction from a radiometric station (for August 2009) or PYR (for year 2014). A day is classified as clear sky, when the average of the hourly cloud fraction shortwave is lower than 5% between 9 UTC and 15 UTC (Sartelet et al., 2018). The other days are considered as cloudy-sky days and

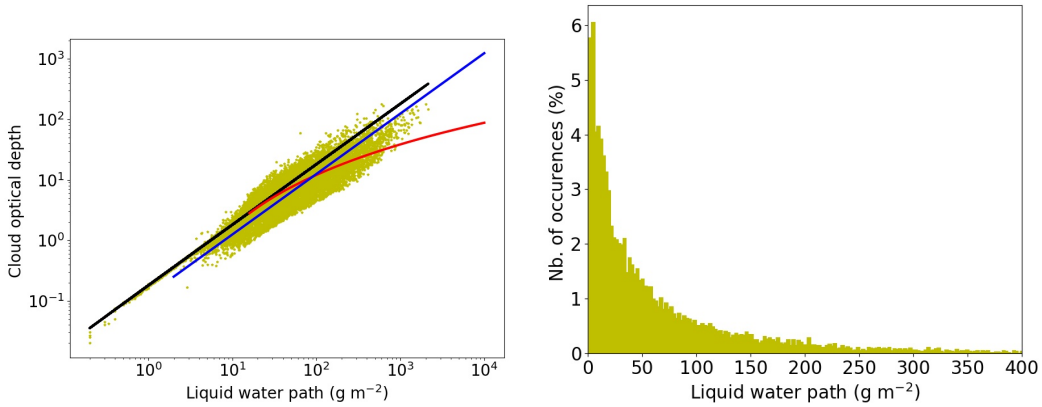

Figure 6: COD versus LWP from 2005 to 2010 at SIRTA (*), the approximation of COD using the fitted model (linear model — + logarithmic model — and equation 1 with r_e=12μm —).

they include overcast skies (cloud fraction higher than 0.95). For every day, only the hours for which all measurements are available are considered. For the case of August 2009, 5 clear-sky days are identified: 6, 12, 15, 16, 23 of August, it is the equivalent of 60 hours, and 20 cloudy-sky days (195 hours). Table 2 shows the number of hours of clear-skies and cloudy-skies for each month of the year 2014. Because only 6 days (75 hours) can be classified as clear sky, the statistical scores are less significant than for cloudy-sky days.

3. Model evaluation

For model evaluation, the computed global and direct irradiances are compared to those measured at the SIRTA site using PYR (see section 2.2.3). The definition of the different statistical indicators used to evaluate our model can be found in appendix C. The different simulations discussed in this paper are reported in Table 3. In the reference simulations used in this section and noted sim09.0 for August 2009 and sim14.0 for the year 2014, the WRF meteorological simulations are used to estimate the COD and the cloud fraction.

3.1. Irradiance on clear-sky days

The model is first evaluated for clear-sky days, which are less numerous than cloudy-sky days, but also easier to model. For August 2009, the daily

Month of year 2014	Nb. of clear-sky hours	Nb. of cloudy-sky hours
January	0	147
February	0	204
March	23	284
April	14	287
May	15	229
June	16	332
July	16	307
August	0	398
September	0	316
October	0	275

Table 2: Number of clear-sky and cloudy-sky hours for each month of 2014 following the availability of cloud fraction from PYR and LWP from radiometric measurements.

Period	Case	Fc	COD
August 2009	Sim09.0	WRF	WRF
	Sim09.1	WRF	Satellite
	Sim09.2	1	Satellite
	Sim09.3	PYR	Satellite
	Sim09.4	Sky imager	Satellite
	Sim09.5	Lidar	Satellite
	Sim09.6	Satellite	Satellite
	Sim09.7	PYR	WRF
Year 2014	Sim14.0	WRF	WRF
	Sim14.1	WRF	Fitted model
	Sim14.2	1	Fitted model
	Sim14.3	PYR	Fitted model
	Sim14.4	Sky imager	Fitted model
	Sim14.5	PYR	Equation 1
	Sim14.6	PYR	WRF

Table 3: Cloud parameters defining the different cases studied. F_C: cloud fraction; COD: cloud optical depth.

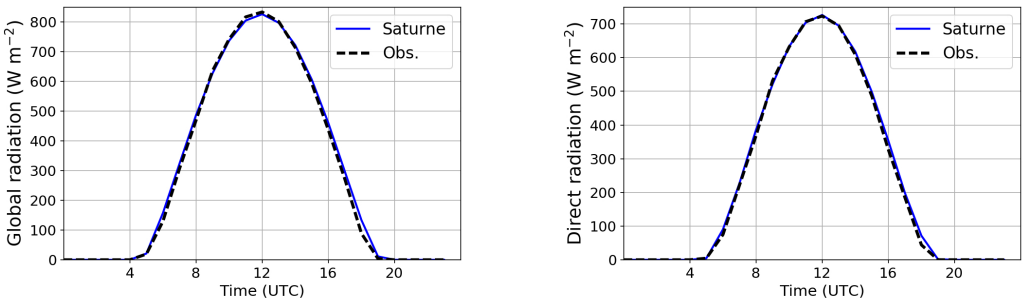

(a) Global irradiance

(b) Direct irradiance

Figure 7: Diurnal cycle of solar irradiances at SIRTA on clear-sky days in August 2009 (in W m^{-2})

global and direct solar irradiances on clear-sky days at SIRTA in August 2009 (Sim09.0) are shown respectively in Figures 7a and 7b. The daily cycle and amplitude are well modelled for both global and direct irradiances. Statistics show a RMSE around 22 W m^{-2} for global irradiance with a MBE of 5 W m^{-2} and a RMSE around 19 W m^{-2} for direct irradiance with a MBE of 5 W m^{-2}.

For the year 2014, the model performs well for global fluxes, although it slightly underestimates the measurements. The RMSE ranges between 12 and 29 W m^{-2} depending on the month, with an average of 19 W m^{-2}and a MBE of 5 W m^{-2} on average. For direct fluxes, the model underestimates the measurements with an averaged MBE of -7 W m^{-2} and the RMSE ranges between 15 and 28 W m^{-2} depending on the month, with an average of 21 W m^{-2}. The estimation of the direct component is less good in 2014 than in August 2009, because aerosol optical depths were estimated from the measurements for August 2009 and from the modelling for the year 2014.

These scores can be compared to the RMSE scores obtained at the BSRN station of Palaiseau using the McClear model, an irradiance model developed for clear-sky conditions (Lefèvre et al., 2013) or to the HelioClim-3v3 database (Blanc et al., 2011; Espinar et al., 2012), which is derived from images of the Meteosat series of satellites. For the period 2005-2007, the McClear model leads to a RMSE of 25 W m^{-2} for global irradiance and of 37 W m^{-2} for direct normal irradiance (Lefèvre et al., 2013); for the HelioClim-3v3 database, the RMSE is equal to 62 W m^{-2} for global irradiance and to 79 W m^{-2} for direct normal irradiance (Espinar et al., 2012).

Although the number of cases, the period and the time averaging period of

our simulation and measurement are not the same as those of Mc Clear/Helioclim-3v3, the scores obtained with code_saturne demonstrate the quality of the model.

3.2. Irradiance on cloudy-sky days

The comparison between observations and simulations during cloudy-sky days in August 2009 is provided in Table 4. As in KS18, Sim09.0 strongly overestimate observations with a RMSE of 149 W m^{-2} and 220 W m^{-2} for global and direct irradiance respectively. The overestimation is larger for the direct than for the global irradiances (MBE=+108 W m^{-2} and NMB of +99% versus +65 W $m^{-2}$and +31%).

As for August 2009, the modelled global and direct irradiances are strongly overestimated during the year 2014 (Table 4; Sim14.0). For global irradiance, the RMSE averaged over the whole year 2014 is 146 W m^{-2} with an averaged MBE of 26 W m^{-2} and a NMB that reaches its maximum of + 49 % in January and its minimum of -7% in June. For direct irradiance, the averaged RMSE is equal to 157 W m^{-2} with a MBE of 23 W m^{-2} and a NMB ranging from +134 % (in January) to +11 % (in July). For both periods, these large errors may come from a bad estimation of cloud fraction and COD. However, statistical scores are slightly better for 2014 than for August 2009, probably because of the lower resolution of WRF simulations in 2009.

4. Improvement of irradiance modelling on cloudy-sky days

In the aim of improving irradiance modelling on cloudy-sky days, different simulations are conducted using observed data for the cloud optical depth and/or the cloud fraction. The simulations are summarized in Table 3.

4.1. Cloud Fraction

The different measurements of cloud fraction (section 2.2.3) and the simple value of 1, sometimes used in modelling (Nielsen et al., 2014), are used as input to the code. They are compared to the cloud fraction extracted from the WRF simulations. In the cases presented here, the COD is taken from satellite measurements for August 2009 and from the fitted model for the year 2014 using radiometric measurements of LWP.

4.1.1. Cloud fraction equals to 1

The modification of cloud fraction (Sim09.2) has an important impact on the estimation of irradiance for August 2009 and especially for the direct irradiance. Taking the cloud fraction equal to 1 leads to an under-estimation of the measurements: the RMSE is equal to 204 W m^{-2}, the MBE to -101 W m^{-2} and the NMB to -67 % (against 203 W m^{-2} , +94 W m^{-2} and +78% respectively for direct irradiance using WRF for the cloud fraction - Sim 09.1- Table 4). A similar behavior is seen for the year 2014 (Sim14.2). The RMSEs, MBEs and NMBes are reported for every month in Figures 8,9 and 10 and the averages over the year for RMSEs and MBEs are in Table 4. Direct fluxes are highly under-estimated for every month (the NMB varies from -99 % (January) to -60% (May), with an averaged MBE of -63 W m^{-2}) and values of RMSE range from 33 to 184 W m^{-2} with an average of 131 W m^{-2}.

For the two simulated periods, the MBEs are high and negative. Due to a significant number of partially cloudy days at SIRTA, taking a cloud fraction of 1 for the whole period leads to a large under-prediction of the direct irradiance. However, it leads to satisfactory results for global irradiance (RMSE=65 W m^{-2}, MBE=+12 W m^{-2}, NMB of +45 % in January and +8 % in May and August), partially justifying its utility in NWP models.

4.1.2. Cloud Fraction extracted from measurements

The computation of irradiances, using measurements for the cloud fraction, improved especially for the direct irradiance. Clouds mainly transform direct irradiance in diffuse irradiance and consequently their impact is lower for global irradiance than for direct irradiance. Statistical scores for August 2009 are reported in Table 4. For the direct irradiance, the best RMSE is obtained using the cloud fraction from PYR (Sim09.3: RMSE of 87 W m^{-2} and NMB of -17 % against 203 W m^{-2} and +79% when the cloud fraction is from WRF simulation - Sim09.1). The estimation of direct irradiance using the cloud fraction from sky imager also leads to similar results, with a RMSE of 99 W $m^{-2}$and a NMB of -27%. However, the direct irradiance is highly under-estimated when the cloud fraction is extracted from the lidar (Sim09.5) and satellite images (Sim09.6), with a MBE score equals, respectively, to -53 W m^{-2} and -40 W m^{-2}, NMB equals, respectively to -50 % and -33% and RMSE equals, respectively, to 135 W m^{-2} and 112 W m^{-2}.

For the year 2014, the statistical scores using the cloud fraction from PYR and sky imager are represented in Figures 8, 9 and 10. With a cloud

fraction from PYR (Sim14.3), the RMSEs for global irradiance range between 37 and 69 W m^{-2}, depending on the month, with an average of 59 W m^{-2} and an average MBE of +17 W m^{-2}. The NMB scores range between +4% and +47%. Global fluxes are always over-estimated. For direct irradiance, the model underestimates the measurements with an averaged MBE of -18 W m^{-2}, a NMB between -22% and -45% and the RMSE ranges between 16 and 88 W m^{-2} depending on the month, with an average of 50 W m^{-2}. Simulations with the cloud fraction extracted from the sky imager (Sim14.4) lead to similar statistics for global radiation and slightly poorer for direct irradiance: the RMSEs range from 17 to 81 W m^{-2} with an average of 60 W m^{-2}, an averaged MBE of -18 W m^{-2} and a NMB between -1.5% and -39%. These statistics are much better than those obtained in the simulations with a cloud fraction from WRF (Sim14.1), which lead to an averaged RMSE for global irradiance of 93 W m^{-2} and of 130 W m^{-2} for direct irradiance. For all conducted tests, acceptable results are obtained for global fluxes but the change of cloud fraction values highly impacts the direct irradiance. However, the direct component is important for different application of solar energy systems, such as concentrating and flat-plate solar systems (Padovan et al., 2014). Hence, a good representation of cloud fraction is crucial. In our case, the best results are obtained with a cloud fraction extracted from PYR or a sky imager.

4.2. Cloud optical depth

In this section, different estimations of the COD are used for August 2009 and year 2014 and are compared to the COD calculated by WRF. The cloud fraction is extracted from PYR.

4.2.1. Satellite measurements

For August 2009, simulations using the COD measured by satellite (Sim09.3) lead to satisfactory results for both global and direct irradiances. Statistics are reported in Table 4. The RMSE is around 87 W m^{-2} for both global and direct irradiance and the MBE scores are respectively equal to -13 W m^{-2} and -22 W m^{-2}. It shows that simulated fluxes under-estimate measurements. Compared to a COD taken from WRF (Sim09.7), it represents a huge improvement.

4.3. Estimation from LWP

For the year 2014, the COD can be computed from microwave radiometric measurements of LWP using 2 models (fitted model (Sim14.3) or equation

	Direct		Global	
Case	RMSE (W m^{-2})	MBE (W m^{-2})	RMSE (W m^{-2})	MBE (W m^{-2})
Sim09.0	220	+108	149	+65
Sim09.1	203	+94	131	+48
Sim09.2	204	-101	103	-32
Sim09.3	87	-22	87	-13
Sim09.4	99	-33	87	-14
Sim09.5	135	-53	94	-23
Sim09.6	112	-40	88	-18
Sim09.7	198	+82	156	+82
Sim14.0	157	+23	146	+26
Sim14.1	130	-6	93	+33
Sim14.2	131	-63	65	+12
Sim14.3	50	-18	59	+17
Sim14.4	60	-18	60	+19
Sim14.5	49	-16	66	+17
Sim14.6	125	+22	131	+25

Table 4: Comparison of simulated and measured direct and global solar irradiances at SIRTA during cloudy days for the different cases studied. The RMSEs and MBEs are expressed in W m^{-2}.

1 (Sim14.5)), as described in section 2.3.2. RMSEs, MBEs and NMBes are respectively reported in Figures 8, 9 and 10. The RMSEs are higher in summer than in winter, because irradiance fluxes are higher. In fact, as it can be seen in Figure 10, relative errors are more important in the winter than in summer (for Sim 14.3: for global irradiance, NMB= +47 % in January and NMB= +4 % in June and for direct irradiance, NMB=-45 % in January and NMB= -22% in June).

The direct irradiance estimated using the COD of the fitted model is mainly described by the linear equation (defined for values of LWP lower than 14 g m^{-2}). This is due to the fact that values of LWP greater than 14 g m^{-2} lead to COD greater than 2.5, and clouds with COD greater than 2.5 are thick enough to lead to very small direct irradiance. The scores are very similar but slightly better when the COD is estimated using equation 1 with a fixed effective radius than using the fitted model.

In opposite to the direct irradiance, which becomes almost zero if clouds have a LWP higher than 14 g m^{-2}, the global irradiance decreases as the COD increases, but it does not cancel out because of diffuse irradiance. Therefore, the global irradiance is impacted by the whole range of values of COD. Similar statistical scores are obtained with the fitted model and using Equation 1 but slightly better scores are obtained with the fitted model (Sim 14.3). For Sim14.3, the lowest RMSE scores, for global irradiance, is equal to 37 W m^{-2} and is obtained in January, and the highest is around 69 W m^{-2}, it is obtained in May. The averaged RMSE is 59 W m^{-2}. For direct irradiance, RMSEs are in the range [16 , 88] W m^{-2}, with an average of 50 W m^{-2}. Therefore, for this case, code_saturne overestimates global irradiance and underestimates direct irradiance for every month of the year 2014.
The results are satisfactory and a big improvement compared to the case when COD is taken from WRF measurements (Sim14.6: the averaged RMSE for global irradiance is about 131 W m^{-2} and for direct irradiance, the RMSE is about 125 W m^{-2}).
This study shows the importance of COD in the estimation of irradiance fluxes during cloudy sky days. It can be well estimated from LWP data (in this case extracted from radiometric measurements) or empirical relations to improve the estimation of irradiance during cloudy-sky days. It also shows the stronger importance of COD compared to the cloud fraction for the estimation of global irradiance.

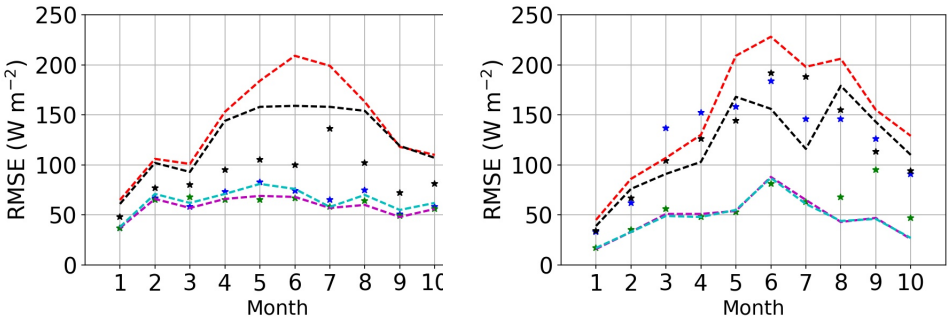

(a) Global irradiance (b) Direct irradiance

Figure 8: RMSEs (in W m^{-2}) between simulated and measured global (a) and direct (b) solar irradiances at SIRTA during cloudy-sky days in 2014. WRF evaluation: - - - Sim14.0. Sensitivity to cloud fraction/COD: * Sim14.1; * Sim14.2;* Sim14.4;- - - Sim14.3; - - - Sim14.5; - - - Sim14.6.

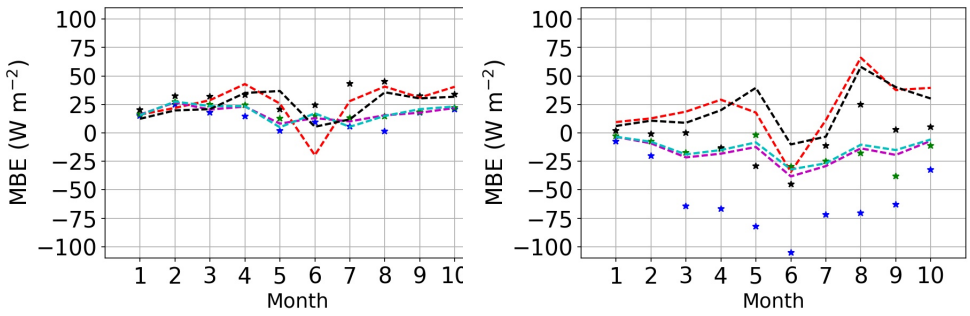

(a) Global irradiance (b) Direct irradiance

Figure 9: MBEs (in W m^{-2}) between simulated and measured global (a) and direct (b) solar irradiances at SIRTA during cloudy-sky days in 2014. WRF evaluation: - - - Sim14.0. Sensitivity to cloud fraction/COD: * Sim14.1; * Sim14.2;* Sim14.4;- - - Sim14.3; - - - Sim14.5; - - - Sim14.6.

5. Discussion

The calculation of irradiance fluxes by code_saturne is done hourly. For the majority of simulated hours, code_saturne approximates well the observations. However, it is not always the case. Thus, an analysis of the results is conducted in order to understand why the quality of the estimation of the

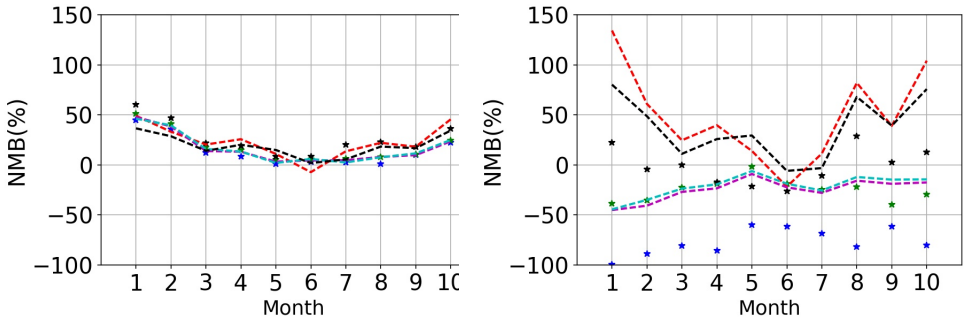

(a) Global irradiance

(b) Direct irradiance

Figure 10: NMB scores (in %) between simulated and measured global (a) and direct (b) solar irradiances at SIRTA during cloudy-sky days in 2014. WRF evaluation: - - - Sim14.0. Sensitivity to cloud fraction/COD: * Sim14.1; * Sim14.2;* Sim14.4;- - - Sim14.3; - - - Sim14.5; - - - Sim14.6.

irradiance varies. The analysis is done for August 2009 (Sim 09.3) and for the year 2014 (Sim14.3). One first explanation of the gap between observation and simulation is that code_saturne calculates the irradiance fluxes at each full hour without integration while the observational data are averaged. In fact, for each variable taken from the SIRTA ReObs file, the hourly mean values are calculated from the native resolution data (5 s to 1 min) by averaging all the data available within ±30 min around the full hour (Chiriaco et al., 2018).

For August 2009, the cases when the absolute difference on global or direct irradiance is higher than 200 W m^{-2} are analysed: 20 hours in 2009 were detected. Among these cases of large differences between simulated and observed direct irradiance, 63% correspond to partially cloudy days and 32% to fully cloudy days. There was no precipitation for any case. In most of the cases, 58%, were obtained when a low cloud was present. 32% of cases were obtained during a transition period of COD: the hour after a minima or maxima of COD.

The analysis is now conducted for the entire simulation of year 2014. The standard deviation of the measured global irradiance, LWP and cloud fraction are extracted from the SIRTA ReObs file. Table 5 shows the MAE of global and direct irradiances for different conditions on the measured global irradiance, LWP and cloud fraction. A better estimation of global irradiance

	MAE(G)	MAE(D)
$\sigma(G_{obs}) > 100$	68	73
$\sigma(G_{obs}) < 100$	25	13
$\sigma(LWP)$ >30	39	16
$\sigma(LWP)$ <30	29	24
$\sigma(F_C) > 0.2$	62	64
$\sigma(F_C) < 0.2$	30	19

Table 5: MAE of global (G) /direct (D) irradiance fluxes (in W m^{-2}) for different ranges of standard variation of measured global irradiance G_{obs}(in W m^{-2})/liquid water path LWP in (g m^{-2}) / cloud fraction F_C in 2014.

	$G_{CS} - G_{obs} < 0$	$G_{CS} - G_{obs} > 0$
$\bar{\sigma}(G_{obs})$	88	32
$\bar{\sigma}(LWP)$	78	41
$\bar{\sigma}(F_C)$	0.086	0.06

Table 6: Averaged standard variation of measured global irradiance G_{obs} (in W m^{-2})/liquid water path LWP (in g m^{-2})/ cloud fraction F_C when measured global irradiance is underestimated or overestimated by code_saturne in 2014.

Condition	$F_c > 0.95$	$0.50 < F_c < 0.75$	$0.25 < F_c < 0.50$
MAE (G)	83	62	43
$\bar{G}_{obs}$	178	452	458
MAE(G)/$\bar{G}_{obs}$	0.46	0.14	0.09
MAE (D)	12	81	75
$\bar{D}_{obs}$	13	239	305
MAE(D)/$\bar{D}_{obs}$	0.92	0.34	0.25

Table 7: Mean absolute error (MAE) of global (G) and direct (D) irradiances and the ratio MAE over the averaged measured fluxes for different conditions on the cloud fraction (F_C) in 2014 (in W m^{-2}).

is obtained for lower fluctuations of measured global irradiance, LWP and cloud fraction. A similar tendency is obtained for direct irradiance except when the standard deviation of LWP is higher than 30 g m^{-2}. It is normal considered that direct irradiance is attenuated for values of LWP higher than 14 g m^{-2}. Therefore, the quality of the estimation is linked to the quick changes within an hour in the measurements.

Table 6 shows the standard variation of measured global irradiance fluxes/ LWP and cloud fraction when measured global irradiance is over-estimated and under-estimated. When code_saturne under-estimates observations, the averaged standard deviation of observed global irradiance, LWP and cloud fraction are higher than when code_saturne overestimates observations. It can be related to the fact that averaging of measurements pushes them towards higher values.

The mean absolute error (MAE) is calculated for the global and direct irradiances for different ranges of cloud fraction in 2014 (table 7). The MAE increases with the cloud fraction. The ratio MAE-mean measured irradiance is higher for the direct irradiance. For overcast situations, diffuse irradiance is dominant. The few high values of simulated direct irradiance during overcast sky are obtained when the COD is low, they might be due to a poorly coordination between measured LWP and cloud fraction or to a low density cloud blocking the sun.

The type of clouds does not contribute significantly to the difference. Cirrus clouds optical depth is usually described by another formula than used here (for ice clouds, the definition of cloud optical proprieties can be found in (Fu, 1996; Baum et al., 2014)). A study was done on hours during which cirrus clouds were the only type of cloud present. It was shown that they are well represented in code_saturne and hourly differences of irradiance fluxes are not linked to their presence.

6. Conclusion

The 1D irradiance model of the atmospheric module of code_saturne was used to calculate irradiance fluxes at SIRTA in Palaiseau, Ile-de-France. This study aimed at improving the estimation of irradiance during cloudy-sky days. Therefore, the model was evaluated hourly and with the presence

of clouds during two periods: August 2009 and year 2014. Cloud properties, such as the cloud fraction and COD, are used as input. Because the mesoscale meteorological model have difficulties to estimate them, measurements done at the SIRTA site were used. The cloud fraction was extracted from satellite images, lidar, shortwave measurements (PYR) and sky imager. The liquid water path (LWP)/COD were extracted from radiometric and satellite measurements. The main conclusions are:

- A good representation of the COD is crucial for modelling solar irradiance during cloudy-sky days. The cloud fraction may improve solar irradiance modelling if the estimation of COD is correct, especially for direct irradiance.

- Assuming the sky completely cloudy but with an accurate representation of COD leads to simulated global irradiance that may be more accurate than using an estimation of cloud fraction from numerical models. However, it is not the case for the direct irradiance.

- The simulated irradiance obtained using a cloud fraction extracted from PYR or from sky imager is more accurate than those obtained using lidar or satellite measurements.

- A fitted model was developed to estimate COD from LWP measurements. Satellite and radiometric measurements of LWP lead to satisfactory simulations of irradiances, although satellite data are not always available. This shows that the link that exists between COD and LWP is well established, and that LWP may be used as a proxy of COD in irradiance modelling.

Moreover, hourly values of solar fluxes were examined to determine the reasons for the few discrepancies between measurements and simulated irradiances. The main source of errors that were detected are:

- code_saturne calculates fluxes every hour, while observational data are averaged within 30 mins around the full hour.

- The hourly bias is higher when the fluctuations within the hour of global irradiance/LWP/cloud fraction measurements are high.

- There was no particular type of clouds that impacted the results. However in August 2009, during more than 50% of the cases leading to a large discrepancy between measurements and observations, a low cloud was present.

- The MAE on irradiance fluxes increases with the cloud fraction and its impact is more important for the direct component.

Overall, we showed that code_saturne performs well at SIRTA during clear-sky and cloudy-sky days, when measurements of cloud fraction and LWP are used. All components of irradiance are well modeled and especially the direct fluxes (with RMSEs around 21 W m^{-2} during clear-sky days and 50 W m^{-2} during cloudy sky-days) which is mandatory for some applications such as concentrating and flat-plate solar systems.

Acknowledgment: The authors would like to acknowledge SIRTA for providing the data used in this study. The work of L. Al Asmar was supported by CEREA, a member of the Pierre-Simon Laplace Institute (IPSL) and by ANRT through an EDF-CIFRE contract (Grant number: 2018/1415).

Appendix A. Calculation of cloud optical properties

The cloud fraction, COD and LWP were extracted from SIRTA Re-Obs data file or WRF simulation. The cloud droplet radii, single scattering albedo (SSA) and asymmetry factor had to be calculated in the code.

Cloud droplet radii. It is calculated following equation 1.

Cloud single scattering albedo (SSA) and the cloud asymmetry factor . The calculations are made separately in the UV-vis band and in the SIR band. They are approximated following the formulations of (Nielsen et al., 2014). They depend only on the equivalent cloud droplets radius r_e, and are defined for different spectral bands: 250-440; 440-690nm in the UV-visible domain and 690-1190; 1190-2380nm in near IR domain. The integration over the wavelength is made by weighting each formulation with the irradiance energy contained in each band. The single scattering albedo (SSA) in the UV-visible and SIR bands (ω_0^{UV-Vis} and ω_0^{SIR})are calculated with the following formulas:

$$\omega_0^{UV-Vis} = \omega_{0-1} \times 0.24 + \omega_{0-2} \times 0.76 \tag{A.1}$$

$$\omega_{0-1} = 1 - 3.3 \times 10^{-8} re \tag{A.2}$$

$$\omega_{0-2} = 1 - 10^{-7} re \tag{A.3}$$

In the SIR band,

$$\omega_0^{SIR} = \omega_{0-3} \times 0.60 + \omega_{0-4} \times 0.40 \tag{A.4}$$

$$\omega_{0-3} = 0.99 - 1.49 \times 10^{-5} re \tag{A.5}$$

$$\omega_{0-4} = 0.9985 - 9.210^{-4} re \tag{A.6}$$

In the UV-Vis band, the cloud asymmetry, g_0^{UV-Vis}, is calculated with the following formula:

$$g_0^{UV-Vis} = \omega_{0-1} \times 0.24 \times g_1 + \omega_{0-2} \times 0.76 \times g_2 \tag{A.7}$$

$$g_{0-1} = 0.868 + 1.4 \times 10^{-4} re - 6.1 \times 10^{-3} e^{-0.25re} \tag{A.8}$$

$$g_{0-2} = 0.868 + 2.5 \times 10^{-4} re - 6.3 \times 10^{-3} e^{-0.25re} \tag{A.9}$$

In the SIR band, the cloud asymmetry, g_0^{SIR}, is calculated with the following formula:

$$g^{SIR} = \omega_{0-3} \times 0.60 \times g_3 + \omega_{0-4} \times 0.40 \times g_4 \tag{A.10}$$

$$g_{0-3} = 0.867 + 3.1 \times 10^{-4} re - 7.8 \times 10^{-3} e^{-0.195re} \tag{A.11}$$

$$g_{0-4} = 0.864 + 5.4 \times 10^{-4} re - 0.133 e^{-0.194re} \tag{A.12}$$

Appendix B. The irradiance model - integral method

Global Irradiance.

UV-Vis band The most significant source of heating in the stratosphere comes from the absorption of solar irradiance by ozone. Rayleigh diffusion through multiple-scattering is taken into account with a simple albedo and the global irradiance G_{UV-VIS}, is expressed as follows:

$$G_{UV-VIS} = F_C G_{1,UV-VIS} + (1 - F_C) G_{2,UV-VIS} \tag{B.1}$$

where F_C is the cloud fraction, $G_{1,UV-VIS}$ and $G_{2,UV-VIS}$ the global irradiance for cloudy-sky and clear-sky with aerosols respectively. They are expressed as:

$$G_{1,UV-VIS} = \mu_0 F_0 (0.647 - \bar{R}_r(\mu_0) - A^G_{UV-VIS}) \frac{T^G_{c,UV-VIS}}{1 - R^G_{c,UV-VIS} R_g} T_{mg} \tag{B.2}$$

$$G_{2,UV-VIS} = \mu_0 F_0 (0.647 - \bar{R}_r(\mu_0) - A^G_{UV-VIS}) \frac{T^G_{a,UV-VIS}}{1 - R^G_{a,UV-VIS} R_g} T_{mg} \tag{B.3}$$

- μ_0 the cosine of the zenith angle
- F_0 the irradiance flux incident at the top of the Earth atmosphere. It is calculated using the formula of (Paltridge and Platt, 1976) : $F_0 = 1365$ W m^{-2}
- $\bar{R}_r$ the albedo due to Rayleigh scattering (as in LH74)
- R_g the ground albedo (calculated by WRF)
- A^G_{UV-VIS} is the irradiance absorption function in the UV-VIS band by O_3 (as in LH74)
- $T^G_{c,UV-VIS}$ and $R^G_{c,UV-VIS}$ the transmission and reflective functions for clouds
- $T^G_{a,UV-VIS}$ and $R^G_{a,UV-VIS}$ the transmission and reflective functions for clear-sky for aerosols
- T_{mg} is the general transmittance function for seven main atmospheric gases (H_2O, O_3, CO_2, CO, N_2O, CH_4 and O_2). It is expressed following (Psiloglou et al., 1997), it depends on 'm', the air mass, given by (Kasten and Young, 1989).

SIR band The most important source of heating in the low atmosphere is due to water vapor absorption. As reported by LH74, parametrizing water vapor absorption is more complicated than for ozone absorption. In the SIR band spectrum, G_{SIR}, is expressed as follows:

$$G_{SIR} = F_C G_{1,SIR} + (1 - F_C) G_{2,SIR} \tag{B.4}$$

where F_C is the cloud fraction; the global irradiance for cloudy-sky $G_{1,SIR}$ and clear-sky with aerosols $G_{2,SIR}$ are expressed as:

$$G_{1,SIR} = \mu_0 F_0 (0.353 - A^G_{SIR}) \frac{T^G_{c,SIR}}{1 - R^G_{c,SIR} R_g} T_{mg} \tag{B.5}$$

$$G_{2,SIR} = \mu_0 F_0 (0.353 - A^G_{SIR}) \frac{T^G_{a,SIR}}{1 - R^G_{a,SIR} R_g} T_{mg} \tag{B.6}$$

- A^G_{SIR} represents the absorption by water vapor (as in LH74)
- $T^G_{c,SIR}$ and $R^G_{c,SIR}$ the transmission and reflective functions for clouds
- $T^G_{a,SIR}$ and $R^G_{a,SIR}$ the transmission and reflective functions for clear-sky for aerosols

The transmission and reflective functions The transmission and reflective functions for cloudy-sky, T^G_c and R^G_c and for clear-sky T^G_a and R^G_a are described by the following formulas of (Meador and Weaver, 1980):

$$T^G = \frac{2k}{(k + \gamma_1) e^{k\tau'} + (k - \gamma_1) e^{-k\tau'}} \tag{B.7}$$

$$R^G = \frac{\gamma_2 [e^{k\tau'} - e^{-k\tau'}]}{(k + \gamma_1) e^{k\tau'} + (k - \gamma_1) e^{-k\tau'}} \tag{B.8}$$

where

$$k = (\gamma_1^2 - \gamma_2^2)^{1/2} \tag{B.9}$$

$$\gamma_1 = \frac{\sqrt{3}}{2} [2 - \omega'_0 (1 + g')] \tag{B.10}$$

$$\gamma_2 = \frac{\sqrt{3} \omega'_0}{2} (1 - g') \tag{B.11}$$

where τ', g' and ω_0' are the scaled optical depths, single scattering albedo and asymmetry factor. They are introduced by (Joseph et al., 1976) in order to take into account the highly forward scattering for water clouds and aerosols (Stephens et al., 1984). This correction is often called δ two-stream(Liou, 2002):

$$\tau' = \tau(1 - \omega_0 * g^2) \tag{B.12}$$

$$\omega_0' = \frac{\omega_0(1 - g^2)}{1 - g^2\omega_0} \tag{B.13}$$

$$g' = \frac{(g - g^2)}{(1 - g^2)} \tag{B.14}$$

The coefficients τ, g and ω_0 change depending if we are on clear-sky or on cloudy-sky conditions:
For clear-sky:

- $\tau = \tau_a$
- $\omega_0 = \omega_a$
- $g = g_a$

For cloudy-sky:

- $\tau = \tau_a + \tau_C$
- $\omega_0 = (\omega_a\tau_a + \omega_C\tau_C)/\tau$
- $g = (g_a\omega_a\tau_a + g_C\omega_C\tau_C)/\tau\omega_0)$

Direct Irradiance. In order to calculate the direct irradiance, a model inspired by LH74 was developed. It is similar to the one developed for global irradiance and it is based on the same principles.

UV-vis band

$$I_{1,UV-VIS} = \mu_0 F_0(0.647 - \bar{R_r} - A^G_{UV-VIS})T_{mg}T^D_C \tag{B.15}$$

$$I_{2,UV-VIS} = \mu_0 F_0(0.647 - \bar{R_r} - A^G_{UV-VIS})T_{mg}T^D_{a,UV-VIS} \tag{B.16}$$

SIR band

$$I_{1,SIR} = \mu_0 F_0 (0.353 - A^G_{SIR}) T_{mg} T^D_C \tag{B.17}$$

$$I_{2,SIR} = \mu_0 F_0 (0.353 - A^G_{SIR}) T_{mg} T^D_{a,SIR} \tag{B.18}$$

where $\mu_0, F_0, \bar{R}_r, A^G$have been defined in the previous paragraphs. $T^D$is given by:

$$T^D = e^{-m\tau} \tag{B.19}$$

Appendix C. Statistical indicators

Different statistical indicators are calculated in this study, they are defined in the following section. o_i and c_i are the observed and the simulated concentrations at time and location i, respectively. n is the number of data. The **Root Mean Square Error (RMSE)**

$$RMSE = \sqrt{\frac{1}{n}\sum_{i=1}^{n}(c_i - o_i)^2} \tag{C.1}$$

The **Mean Fractional Bias Error (MFBE)**

$$MFBE = \frac{1}{n}\sum_{i=1}^{n}\frac{c_i - o_i}{(c_i + o_i)/2} \tag{C.2}$$

The **Mean Bias Error (MBE)**

$$MBE = \frac{1}{n}\sum_{i=1}^{n}(c_i - o_i) \tag{C.3}$$

The **Mean Fractional Error (MFE)**

$$MFE = \frac{1}{n}\sum_{i=1}^{n}\frac{|c_i - o_i|}{(c_i + o_i)/2} \tag{C.4}$$

The **Mean Absolute Error (MAE)**

$$MAE = \frac{1}{n}\sum_{i=1}^{n}|c_i - o_i| \tag{C.5}$$

The **Normalized Mean Bias (NMB)**

$$NMB = \frac{\sum_{i=1}^{n}(c_i - o_i)}{\sum_{i=1}^{n} o_i} \tag{C.6}$$

References

E. Lorenz, D. Heinemann, Prediction of Solar Irradiance and Photovoltaic Power, volume 1, 2012, pp. 239–292. doi:10.1016/B978-0-08-087872-0.00114-1.

M. Diagne, M. David, P. Lauret, J. Boland, N. Schmutz, Review of solar irradiance forecasting methods and a proposition for small-scale insular grids, Renew. Syst. Energ. Rev. 27 (2013) 65–76. doi:10.1016/j.rser.2013.06.042.

G. Reikard, Predicting solar radiation at high resolutions: A comparison of time series forecasts, Sol. Energy 83 (2009) 342–349. doi:10.1016/j.solener.2008.08.007.

S. Cao, J. Cao, Forecast of solar irradiance using recurrent neural networks combined with wavelet analysis, Appl. Therm. Eng. 25 (2005) 161–172. doi:10.1016/j.applthermaleng.2004.06.017.

C. Rigollier, O. Bauer, L. Wald, On the clear sky model of the esra - european solar radiation atlas - with respect to the heliosat method, Sol. Energy 68 (2000) 33–48. doi:10.1016/S0038-092X(99)00055-9.

Y. Xie, M. Sengupta, J. Dudhia, A fast all-sky radiation model for solar applications (farms): Algorithm and performance evaluation, Sol. Energy 135 (2016) 435–445. doi:10.1016/j.solener.2016.06.003.

R. Müller, K.-F. Dagestad, P. Ineichen, M. Schroedter-Homscheidt, S. Cros, D. Dumortier, R. Kuhlemann, J. Olseth, G. Izquierdo, C. Reise, L. Wald, D. Heinemann, Rethinking satellite-based solar irradiance modelling: The solis clear-sky module, Remote Sens. Environ. (2004) 160–174. doi:10.1016/j.rse.2004.02.009.

P. Ineichen, Comparison of eight clear sky broadband models against 16 independent data banks, Sol. Energy 80 (2006) 468–478. doi:10.1016/j.solener.2005.04.018.

S. Clough, M. Shephard, E. Mlawer, J. Delamere, M. Iacono, K. Cady-Pereira, S.-A. Boukabara, P. Brown, Atmospheric radiative transfer modeling: A summary of the aer codes, J. Quant. Spectrosc. Radiat. Transf. 91 (2005) 233–244. doi:10.1016/j.jqsrt.2004.05.058.

K. Stamnes, S.-C. Tsay, W. Wiscombe, K. Jayaweera, Numerically stable algorithm for discrete-ordinate-method radiative transfer in multiple scattering and emitting layered media, Appl. Opt. 27 (1988) 2502–2509. doi:10.1364/AO.27.002502.

H. Breitkreuz, M. Schroedter-Homscheidt, T. Holzer-Popp, S. Dech, Short-Range Direct and Diffuse Irradiance Forecasts for Solar Energy Applications Based on Aerosol Chemical Transport and Numerical Weather Modeling, J. Appl. Meteorol. Climatol. 48 (2009) 1766–1779. doi:10.1175/2009JAMC2090.1.

K. Sartelet, C. Legorgeu, L. Lugon, Y. Maanane, L. Musson-Genon, Representation of aerosol optical properties using a chemistry transport model to improve solar irradiance modelling, Sol. Energy 176 (2018) 439–452. doi:10.1016/j.solener.2018.10.017.

A. Padovan, D. Del Col, V. Sabatelli, D. Marano, Dni estimation procedures for the assessment of solar radiation availability in concentrating systems, Energy Procedia 57 (2014). doi:10.1016/j.egypro.2014.10.100.

C. Bertrand, G. Vanderveken, M. Journée, Evaluation of decomposition models of various complexity to estimate the direct solar irradiance over Belgium, Renew. Energy 74 (2015) 618–626. doi:10.1016/j.renene.2014.08.

J. Polo, L. Martín Pomares, J. Vindel, Correcting satellite derived dni with systematic and seasonal deviations: Application to india, Renew. Energy 80 (2015) 238–243. doi:10.1016/j.renene.2015.02.031.

B. E. Psiloglou, H. D. Kambezidis, Performance of the meteorological radiation model during the solar eclipse of 29 March 2006, Atmos. Chem. Phys. 7 (2007) 6047–6059. doi:https://doi.org/10.5194/acp-7-6047-2007.

P. Blanc, B. Gschwind, M. Lefèvre, L. Wald, The helioclim project: Surface solar irradiance data for climate applications, Remote Sens. 3 (2011) 343–361. doi:10.3390/rs3020343.

M. Lefèvre, A. Oumbe, P. Blanc, B. Espinar, B. Gschwind, Z. Qu, L. Wald, M. Schroedter-Homscheidt, C. Hoyer-Klick, A. Arola, A. Benedetti, J. W. Kaiser, J.-J. Morcrette, Mcclear: A new model estimating downwelling

815 solar radiation at ground level in clear-sky conditions, Atmos. Meas. Tech
816 6 (2013) 2403–2418. doi:10.5194/amt-6-2403-2013.

817 H. Kambezidis, B. Psiloglou, D. Karagiannis, U. Dumka, D. Kaskaoutis,
818 Recent improvements of the meteorological radiation model for solar irra-
819 diance estimates under all-sky conditions, Renew. Energy 93 (2016) 142 –
820 158. doi:10.1016/j.renene.2016.02.060.

821 J.-J. Morcrette, Radiation and cloud radiative properties in the european
822 centre for medium range weather forecasts forecasting system, J. Geophys.
823 Res. Atmos. 96 (1991) 9121–9132. doi:10.1029/89JD01597.

824 J.-J. Morcrette, H. W. Barker, J. N. S. Cole, M. J. Iacono, R. Pin-
825 cus, Impact of a New Radiation Package, McRad, in the ECMWF In-
826 tegrated Forecasting System, Mon. Wea. Rev. 136 (2008) 4773–4798.
827 doi:10.1175/2008MWR2363.1.

828 P. Räisänen, Effective longwave cloud fraction and maximum-random overlap
829 of clouds:a problem and a solution, Mon. Wea. Rev. 126 (1998) 3336–3340.
830 doi:10.1175/1520-0493(1998)126<3336:ELCFAM>2.0.CO;2.

831 G. L. Stephens, Radiation Profiles in Extended Water Clouds. II: Param-
832 eterization Schemes, J. Atmos. Sci. 35 (1978) 2123–2132. doi:10.1175/
833 1520-0469(1978)035<2123:RPIEWC>2.0.CO;2.

834 G. Stephens, S. Ackerman, E. Smith, A shortwave parameterization revised
835 to improve cloud absorption, J. Atmos. Sci. 41 (1984) 687–690. doi:10.
836 1175/1520-0469(1984)041<0687:ASPRTI>2.0.CO;2.

837 K. P. Nielsen, E. Gleeson, L. Rontu, Radiation sensitivity tests of the
838 harmonie 37h1 nwp model, Geosci. Model Dev. 7 (2014) 1433–1449.
839 doi:10.5194/gmd-7-1433-2014.

840 C. M. Naud, A. D. D. Genio, M. Bauer, W. Kovari, Cloud vertical dis-
841 tribution across warm and cold fronts in cloudsat–calipso data and a
842 general circulation model, J. Climate 23 (15 Jun. 2010) 3397 – 3415.
843 doi:10.1175/2010JCLI3282.1.

844 J. M. Haynes, C. Jakob, W. B. Rossow, G. Tselioudis, J. Brown, Major char-
845 acteristics of southern ocean cloud regimes and their effects on the energy
846 budget, J. Climate 24 (2011) 5061 – 5080. doi:10.1175/2011JCLI4052.1.

847 E. Gregow, A. Lindfors, S. van der Veen, D. Schoenach, S. de Haan,
848 M. Lindskog, The use of satellite and surface observations for initial-
849 izing clouds in the harmonie nwp model., Meteorol. Appl. 27 (2020).
850 doi:10.1002/met.1965.

851 C. Schillings, H. Mannstein, R. Meyer, Operational method for deriving
852 high resolution direct normal irradiance from satellite data, Sol. Energy
853 76 (2004) 475 – 484. doi:10.1016/j.solener.2003.07.038.

854 C. Gautier, G. Diak, S. Masse, A simple physical model to estimate incident
855 solar radiation at the surface from goes satellite data, J. Applied Meteor.
856 19 (1980) 1005–1012. doi:10.1175/1520-0450(1980)019<1005:ASPMTE>
857 2.0.CO;2.

858 F. Kurzrock, S. Cros, F. C. Ming, J. A. Otkin, A. Hutt, L. Linguet, G. Lajoie,
859 R. Potthast, A review of the use of geostationary satellite observations in
860 regional-scale models for short-term cloud forecasting, Meteorol. Z. 27
861 (2018) 277–298. doi:10.1127/metz/2018/0904.

862 G. Roy, S. Hayman, W. Julian, Sky analysis from ccd images:
863 cloud cover, Light. Res. Technol. 33 (2001) 211–221. doi:10.1177/
864 136578280103300402.

865 A. Moncada, W. Richardson, R. Vega-Avila, Deep learning to forecast solar
866 irradiance using a six-month utsa skyimager dataset, Energies 11 (2018)
867 1988. doi:10.3390/en11081988.

868 K. Sartelet, S. Zhu, S. Moukhtar, M. André, V. Andre, J.M.and Gros,
869 O. Favez, M. Brasseur, A.and Redaelli, Emission of intermediate, semi
870 and low volatile organic compounds from traffic and their impact on sec-
871 ondary organic aerosol concentrations over greater paris., Atmos. Environ.
872 (2018) 126–137. doi:doi:10.1016/j.atmosenv.2018.02.031.

873 M. André, K. Sartelet, S. Moukhtar, A. J.M., R. M., Diesel, petrol or electric
874 vehicles: what choices to improve urban air quality in the ile-de-france
875 region? a simulation platform and case study., Atmos. Environ. (2020)
876 117752. doi:10.1016/j.atmosenv.2020.117752.

877 M. Haeffelin, L. Barthès, O. Bock, C. Boitel, S. Bony, D. Bouniol, H. Chepfer,
878 M. Chiriaco, J. Cuesta, J. Delanoë, P. Drobinski, J.-L. Dufresne, C. Fla-

mant, M. Grall, A. Hodzic, F. Hourdin, F. Lapouge, Y. Lemaître, A. Mathieu, Y. Morille, C. Naud, V. Noël, W. O'Hirok, J. Pelon, C. Pietras, A. Protat, B. Romand, G. Scialom, R. Vautard, Sirta, a ground-based atmospheric observatory for cloud and aerosol research, Annales Geophysicae 23 (2005) 253–275. doi:10.5194/angeo-23-253-2005.

A. A. Lacis, J. Hansen, A Parameterization for the Absorption of Solar Radiation in the Earth's Atmosphere, J. Atmos. Sci. 31 (1974) 118–133. doi:10.1175/1520-0469(1974)031<0118:APFTAO>2.0.CO;2.

C. Skamarock, B. Klemp, J. Dudhia, O. Gill, D. Barker, G. Duda, X.-y. Huang, W. Wang, G. Powers, A description of the advanced research wrf version 3 (2008). doi:10.5065/D68S4MVH.

J. S. Kain, J. M. Fritsch, Convective Parameterization for Mesoscale Models: The Kain-Fritsch Scheme, American Meteorological Society, Boston, MA, 1993, pp. 165–170. doi:10.1007/978-1-935704-13-3_16.

E. Kessler, On the continuity and distribution of water substance in atmospheric circulations, Atmos. Res. 38 (1995) 109 – 145. doi:10.1016/0169-8095(94)00090-Z.

G. Grell, D. Devenyi, A generalized approach to parameterizing convection combining ensemble and data assimilation techniques, Geophys. Res. Lett. 29 (2002). doi:10.1029/2002GL015311.

M. Chiriaco, J.-C. Dupont, S. Bastin, J. Badosa, J. Lopez, M. Haeffelin, H. Chepfer, R. Guzman, ReOBS: a new approach to synthesize long-term multi-variable dataset and application to the SIRTA supersite, Earth Syst. Sci. Data 10 (2018) 919–940. doi:10.5194/essd-10-919-2018.

J. W. Boylan, A. G. Russell, Pm and light extinction model performance metrics, goals, and criteria for three-dimensional air quality models, Atmos. Environ. 40 (2006) 4946 – 4959. doi:10.1016/j.atmosenv.2005.09.087, special issue on Model Evaluation: Evaluation of Urban and Regional Eulerian Air Quality Models.

B. Holben, T. Eck, I. Slutsker, D. Tanré, J. Buis, A. Setzer, E. Vermote, J. Reagan, Y. Kaufman, T. Nakajima, F. Lavenu, I. Jankowiak, A. Smirnov, Aeronet—a federated instrument network and data archive

for aerosol characterization, Remote Sens. Environ. 66 (1998) 1 – 16. doi:10.1016/S0034-4257(98)00031-5.

C. N. Long, T. P. Ackerman, K. L. Gaustad, J. N. S. Cole, Estimation of fractional sky cover from broadband shortwave radiometer measurements, J. Geophys. Res. Atmos. 111 (2006). doi:10.1029/2005JD006475.

C. N. Long, J. J. DeLuisi, Development of an automated hemispheric sky imager for cloud fraction retrievals, In Proceedings 10th Symposium on Meteorological Observations and Instrumentation, 11–16 January 1998, Phoenix, AZ, USA (1998).

Y. Morille, M. Haeffelin, P. Drobinski, J. Pelon, STRAT: An Automated Algorithm to Retrieve the Vertical Structure of the Atmosphere from Single-Channel Lidar Data, J. Atmos. Ocean. Technol. 24 (2007) 761–775. doi:10.1175/JTECH2008.1.

R. Roebeling, A. Feijt, P. Stammes, Cloud property retrievals for climate monitoring: Implications of differences between SEVIRI on METEOSAT-8 and AVHRR on NOAA-17, J. Geophys. Res. 111 (2006) D20210. doi:10.1029/2005JD006990.

T. Rose, S. Crewell, U. Löhnert, C. Simmer, A network suitable microwave radiometer for operational monitoring of the cloudy atmosphere, Atmos. Res. 75 (2005) 183 – 200. doi:10.1016/j.atmosres.2004.12.005, cLIWA-NET: Observation and Modelling of Liquid Water Clouds.

C. Stubenrauch, Assessment of Global Cloud Datasets from Satellites: Project and Database Initiated by the GEWEX Radiation Panel., Bull. Amer. Meteor. Soc. 94 (2013) 1031–1049. doi:10.1175/BAMS-D-12-00117.1.

B. Espinar, P. Blanc, L. Wald, B. Gschwind, L. Ménard, E. Wey, C. Thomas, L. Saboret, HelioClim-3: a near-real time and long-term surface solar irradiance database, in: Workshop on "Remote Sensing Measurements for Renewable Energy", Risoe, Denmark, 2012. URL: https://hal-mines-paristech.archives-ouvertes.fr/hal-00741564.

Q. Fu, An accurate parameterization of the solar radiative properties of cirrus clouds for climate models, J. Climate 9 (1996) 2058–2082. doi:10.1175/1520-0442(1996)009<2058:AAPOTS>2.0.CO;2.

B. A. Baum, P. Yang, A. J. Heymsfield, A. Bansemer, B. H. Cole, A. Merrelli, C. Schmitt, C. Wang, Ice cloud single-scattering property models with the full phase matrix at wavelengths from 0.2 to 100µm, J. Quant. Spectrosc. Radiat. Transf. 146 (2014) 123 – 139. doi:10.1016/j.jqsrt.2014.02.029, electromagnetic and Light Scattering by Nonspherical Particles XIV.

G. W. Paltridge, C. M. R. Platt, Radiative processes in meteorology and climatology, Elsevier Scientific Pub. C., 1976. doi:10.1002/qj.49710343713.

B. E. Psiloglou, M. Santamouris, D. N. Asimakopoulos, Predicting the spectral and broadband aerosol transmittance in the atmosphere for solar radiation modelling, Renew. Energy 12 (1997) 259–279. doi:10.1016/S0960-1481(97)00044-X.

F. Kasten, A. T. Young, Revised optical air mass tables and approximation formula, Appl. Opt. 28 (1989) 4735–4738. doi:10.1364/AO.28.004735.

W. E. Meador, W. R. Weaver, Two-Stream Approximations to Radiative Transfer in Planetary Atmospheres: A Unified Description of Existing Methods and a New Improvement, J. Atmos. Sci. 37 (1980) 630–643. doi:10.1175/1520-0469(1980)037<0630:TSATRT>2.0.CO;2.

J. H. Joseph, W. J. Wiscombe, J. A. Weinman, The delta-eddington approximation for radiative flux transfer, J. Atmos. Sci. 33 (1976) 2452 – 2459. doi:10.1175/1520-0469(1976)033<2452:TDEAFR>2.0.CO;2.

K. Liou, An Introduction to Atmospheric Radiation, ISSN, Elsevier Science, 2002. URL: https://books.google.fr/books?id=mQ1DiDpX34UC.

Highlights

Improvement of solar irradiance modelling during cloudy-sky days using measurements

Léa Al Asmar, Luc Musson-Genon, Eric Dupont, Jean-Charles Dupont, Karine Sartelet

- Parameterised global irradiance modelling is improved by using measurements of cloud optical depth (COD) only
- Liquid water path is a good-enough proxy to determine COD
- Measurements of cloud fraction are useful if COD is well estimated
- A good representation of cloud fraction is crucial for the estimation of direct irradiance